US Department of Energy, National Energy Technology Laboratory

Contract No. DEEE0007807

High Conductivity and Flexible Hybrid Solid State Electrolyte

Final Report

Submission Date: December 19, 2019

PI: **Eric D. Wachsman, Ph.D.**
Director, University of Maryland Energy Research Center William L. Crentz Centennial Chair in Energy Research University of Maryland
College Park, MD 20742
ewach@umd.edu
Tel.: (301) 405-8193, Fax.: (301)314-8514

Submitting Official: **Stephanie M. Swann**
Contract Manager
University of Maryland
Office of Research Administration 3112
Lee Building 7809 Regents Drive
College Park, MD 20742
oraa@umd.edu
Tel.: (301) 405-6269, Fax.: (301)314-9569

Digitally signed by Stephanie Swann
Date: 2019.12.19 16:11:41 -05'00'
Signature

DUNS Number: **790934285**

High Conductivity and Flexible Hybrid Solid State Electrolyte

Final Report

Eric Wachsman, Principal Investigator
Organization: University of Maryland
Address: 1206 Engineering Laboratory Building
College Park, MD 20742
Phone: (301) 405-8193
E-mail: ewach@umd.edu

Tien Duong, DOE Program Manager
Energy Storage R&D
Office of Vehicle Technologies
U.S. Department of Energy
Washington, DC 20585
Phone: (202) 586-7836
E-mail: Tien.Duong@ee.doe.gov

Start Date: October 2016 End Date: September 2019

Project Introduction

Metallic lithium is considered the "Holy Grail" for high-energy density batteries. However, using lithium metal in organic liquid electrolyte systems faces many challenges in terms of battery performance and safety. A fundamental strategy is to develop a solid-state electrolyte (SSE) to mechanically suppress lithium dendrites and intrinsically eliminate SEI formation. Among the different types of SSEs, solid-polymer electrolytes have been the most extensively studied. In polymer-based composite SSEs, nanoparticles are incorporated to influence the recrystallization kinetics of the PEO polymer chains to promote local amorphous regions, thereby increasing the ionic conductivity of the Li salt/polymer system. The fillers can be either non-Li^+ conductive nanoparticles, such as Al_2O_3, SiO_2, TiO_2, ZrO_2, and organic polymer spheres, or Li^+ conductive nanoparticles, such as $Li_{0.33}La_{0.557}TiO_3$, and $Li_{1.3}Al_{0.3}Ti_{1.7}(PO_4)_3$. Developing nanostructured fillers is an essential approach to increase the ionic conductivity of composite electrolytes due to the increased surface area of the amorphous region and improved interface between fillers and polymers. Meanwhile, numerous solid-state inorganic Li^+ electrolytes are being investigated to replace liquid organic electrolytes. Due to their high ion conductivity and excellent stability, Li-stuffed garnets exhibit the most promising physical and chemical properties for SSEs. However, major challenges still exist in garnet-based electrolytes, including: (1) Being either too thick with corresponding high ASR or too mechanically fragile when thin (~20 μm); (2) High temperature processing that is incompatible with most anode/cathode materials; and (3) High interfacial impedance. Moreover, flexible SSEs with high ionic conductivity and excellent processability are completely lacking.

Recently, the PIs at the University of Maryland (UMD) have pioneered thin garnet based solid state batteries that effectively address the interfacial impedance using gel/polymer layers and here

propose to integrate these two materials (garnet and organic) to address the other issues. We have demonstrated the ability to overcome the solid-electrolyte/solid-electrode interfacial impedance using gel and polymer interfacial layers with solid-state garnet (e.g. $Li_7La_3Zr_2O_{12}$ LLZO) electrolytes under BMR contract DEEE0006860. We now are extending this to an integrated high-conductivity, conformal/flexible and low-interfacial impedance, hybrid (garnet-organic) solid electrolyte. Our approach is based on a continuous network of high-conductivity one-dimensional (1D) garnet electrolyte nanofibers that not only provide greater conductivity, but through microstructural optimization can block Li-dendrite propagation. We have already demonstrated the ability to synthesize 1D garnet nanofibers by electrospinning and that the corresponding hybrid electrolyte (after infiltrating the pore structure with a polymer electrolyte) is flexible with enhanced mechanical properties compared to the polymer matrix. Moreover, it has greater thermal stability than the polymer alone, high ion conductivity, excellent stability with Li metal and can be used to make solid-state metal anode batteries with S cathode, as well as low electrode interfacial impedance due to the intrinsic gel/polymer-interface developed in the current BMR project. Therefore, this can potentially revolutionize solid-state, metal-anode, battery technology.

Instability and/or high resistance at the interface of lithium metal with various solid electrolytes limit the use of the metallic anode for batteries with high energy density, such as Li-air and Li-S batteries. The critical impact of this endeavor will be focused on developing a new type of solid-state electrolyte (SSE) that is highly conductive, highly flexible and electrochemically stable. In particular, the new SSE will enable Li metal anodes with excellent interfacial impedance and blocking formation of Li dendrites.

Objectives

The project objective is to develop flexible hybrid electrolyte with garnet nanofibers to achieve the following: (1) flexiblity, with greater mechanical strength (~ 10 MPa) and thermal stability than polymer electrolytes; (2) high room-temperature ionic conductivity, ~ 0.5 mS/cm; (3) stable interface with lithium metal and effective blocking of lithium dendrites at current densities up to 3 mA/cm^2; and (4) battery performance with Li-S chemistry with an energy density of ≥ 450 Wh/kg (and ≥ 1000 Wh/L) and maintaining ≥ 80% of capacity up to 500 cycles.

Approach

We synthesized garnet nanofibers, filled the porous region with polymer electrolyte, and characterized and tuned the flexible hybrid membrane properties. The flexible hybrid SSE microstructure was analyzed by leveraging the UMD AIMLab Focused Ion Beam Scanning Electron Microscopy (FIB-SEM) tools and integrated with electrochemical methods at the UMERC Battery Fabrication Lab to investigate the properties and stability with Li metal anode. We developed a fundamental understanding of the mechanism of Li ionic diffusion in garnet nanofibers and their mechanical properties, as well as these properties for hybrid garnet-fiber/polymer hybrids. Work progressed toward the study of the electrode assembly during electrochemical cycling of the anode.

Results

1. Fabrication of Hybrid Electrolyte

1.1. Electrospinning fabrication of garnet nanofiber membrane

Stoichiometric amounts of chemicals were dissolved in Dimethylformamide (DMF) with acetic acid. 10% excess $LiNO_3$ was added to compensate for lithium volatilization during high temperature synthesis. The salt solution and polyvinylpyrrolidone (PVP) in DMF (10%) solution were mixed at a 1:1 volume ratio to form a precursor solution for electrospinning. The electrospinning setup was composed of a syringe pump, a high voltage power supply, and a drum collector covered with aluminum foil.

After electrospinning, the as-spun fiber membrane was peeled off the collector and placed in an alumina crucible for calcination. The calcination process was conducted in air at 800 °C for 4 h to remove PVP polymer and crystalize the fibers. Figure 1 shows the morphology of Garnet nanofibers before and after sintering. The as-spun membrane consists of continuous nanofibers with diameters ranging from ~200 to 300 nm. After calcination, PVP polymer was removed and garnet nanofibers were crystalized (Figure 1).

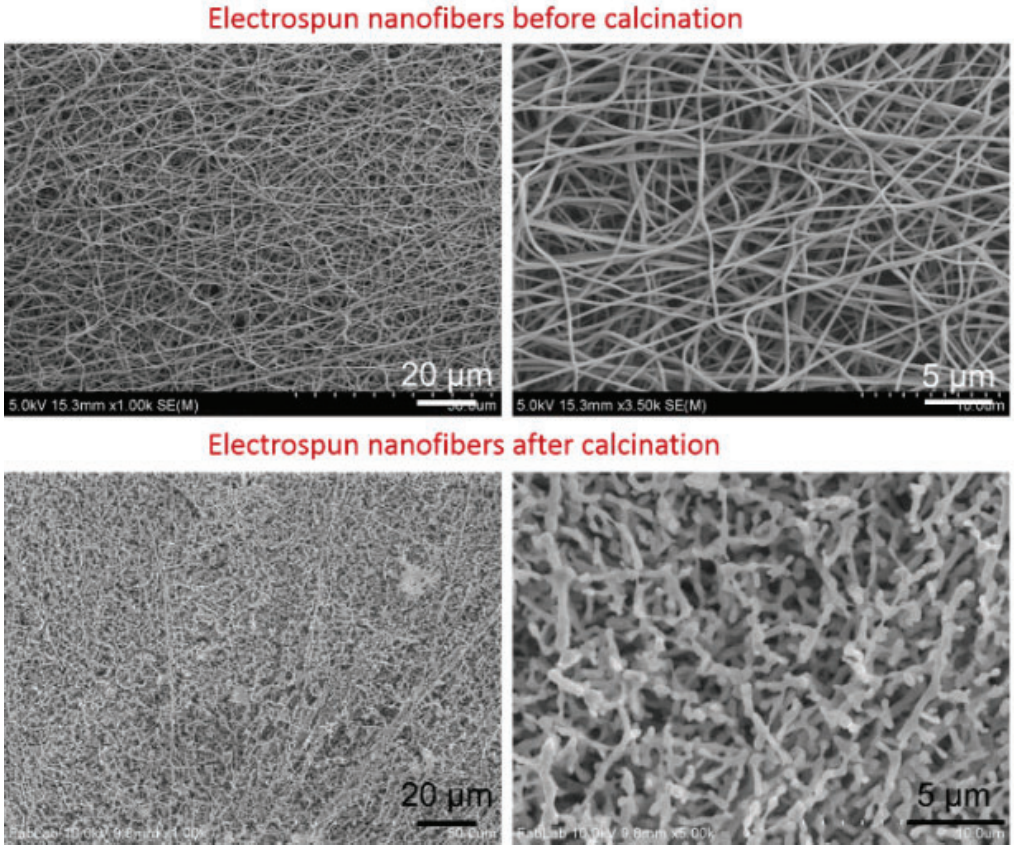

Figure 1. SEM images of garnet nanofibers before and after calcination.

PEO-LiTFSI was filled into the garnet nanofiber membrane by repeated wetting and drying to get flexible solid-state membrane. The total lithium ion conductivity of flexible solid-state electrolyte

was characterized by electrochemical impedance spectroscopy (EIS). Figure 2 shows the Arrhenius plot of the garnet nanofiber electrolyte conductivity. Lithium ion conductivity was calculated based on the thickness FRPC electrolyte and diameter of stainless electrodes. Lithium ion conductivity of cubic phase LLZO garnet pellet would reach as high as 10^{-3} S/cm, while lithium salt stuffed PEO is generally in the order of 10^{-6}-10^{-9} S/cm at room temperature. Our flexible electrolyte combining conductive cubic LLZO garnet and lithium-PEO exhibited reasonably high ionic conductivity of 2.5×10^{-4} S/cm at room temperature.

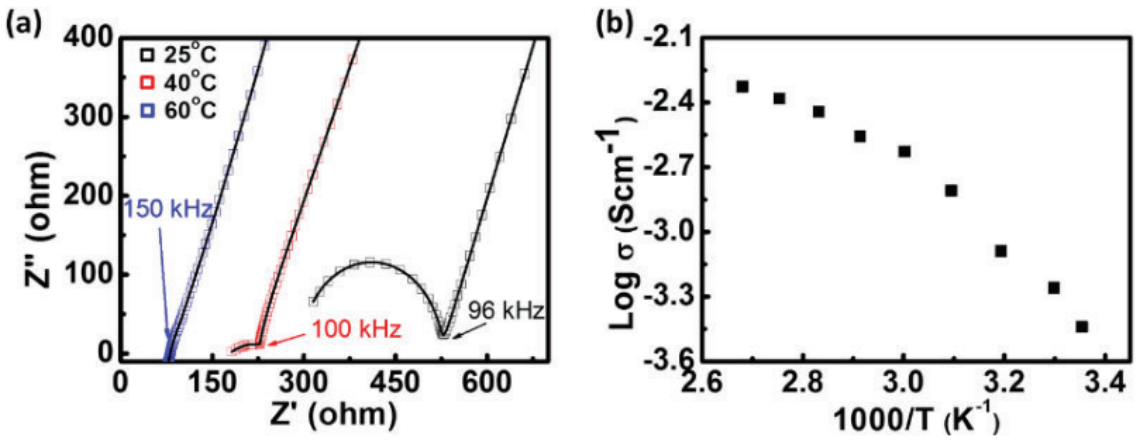

Figure 2. (a) EIS profiles of the flexible electrolyte membrane at different temperatures (25°C, 40°C, and 90°C). (b) Arrhenius plot of the flexible electrolyte membrane at elevated temperatures.

1.2. Fabrication of 4 cm by 4 cm garnet nanofiber membrane from templates

A very scalable method was developed to produce large-size garnet nanofiber membranes. Al-doped LLZO with the chemical composition of $Li_{6.28}Al_{0.24}La_3Zr_2O_{11.98}$ was prepared by dissolving stoichiometric amounts of $LiNO_3$ (99%; Alfa Aesar), $Al(NO_3)_3{\bullet}9H_2O$ (98%; Alfa Aesar), $La(NO_3)_3{\bullet}6H_2O$ (99.9%; Alfa Aesar), and Zirconium propoxide solution (70 wt.%; Sigma Aldrich) in ethanol with 15 vol % acetic acid. Excess $LiNO_3$ (15 wt.%) was added to compensate for lithium loss during the subsequent calcination procedure. Cellulose textile templates were pretreated by annealing in air at 270 °C for 10 h, then rinsed with ethanol (Sigma Aldrich) and dried at 100 °C for 12 h. After pretreatment, the templates were soaked in a 2.5 mol/L LLZO precursor solution for 24 h. The multi-scale porosity existing in the porous templates enabled homogenous impregnation by the LLZO precursor. Calcination of the precursor impregnated templates was conducted in oxygen at different temperatures to obtain garnet fibrous membrane. Figure 3 shows the photograph of the garnet fibrous membrane sintered at 800 °C, which essentially retained the characteristic physical features of the original cellulose template and can be tailored for particular shapes in large dimensions (4cm × 4cm).

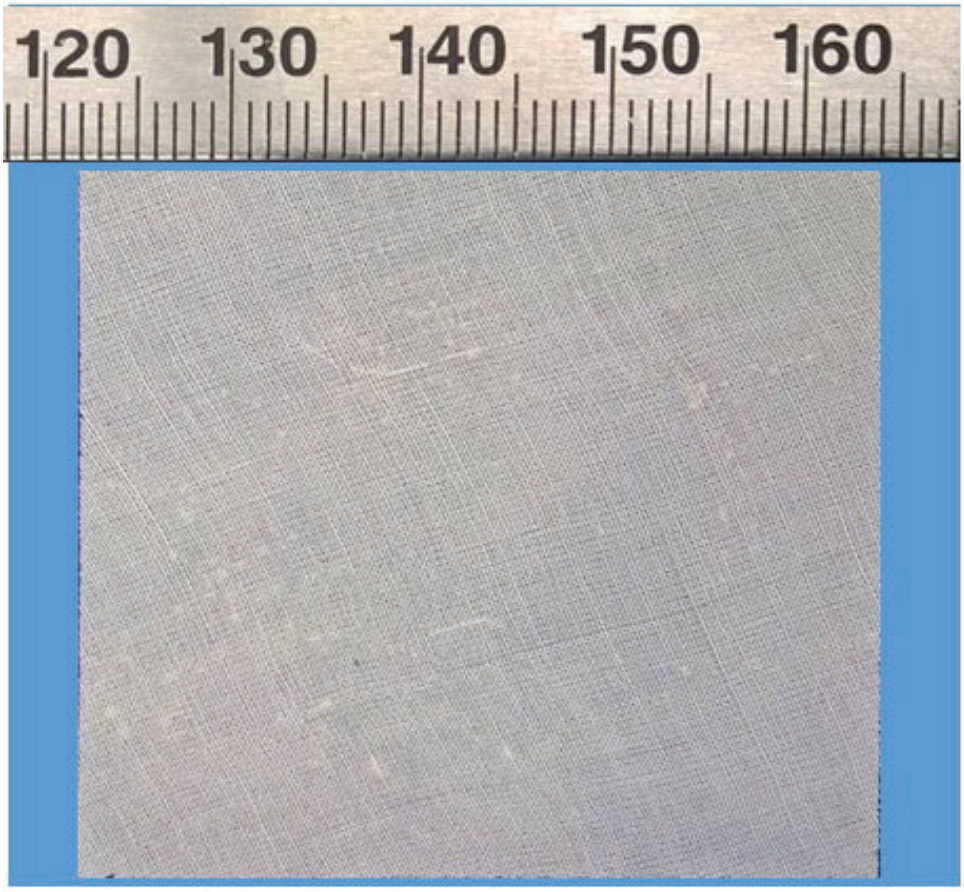

Figure 3. Photograph of 4cm × 4cm flexible garnet fibrous membrane

The crystallographic phase of the LLZO was analyzed by powder X-ray diffraction on a D8 Advanced with LynxEye and SolX (XRD, Bruker AXS) using a Cu Kα radiation source operated at 40 kV and 40 mA. The microstructure and element distribution were examined by analytical scanning electron microscope (SEM, Hitachi SU-70) equipped with an Energy Dispersive Spectrometer (EDS, Oxford Instruments). Figure 4 shows the XRD pattern and SEM image of garnet fibrous membrane. Through simple composition design by doping with supervalent cations and optimizing lithium concentration in the precursor solution, stabilization of the cubic phase was achieved at sintering temperatures as low as 800 °C. The garnet fibers retained the characteristic physical features of the original template, which consisted of continuous individual microfibers of approximately 10 μm in diameter that were arranged mostly parallel and twisted around each other. The fibers were wrapped into bundles about 200 μm in diameter interlacing with each other to form the periodically ordered woven pattern. Inter-fiber pores ranged from 10 to 20 μm in diameter and larger pores between yarns were formed after thermal treatment.

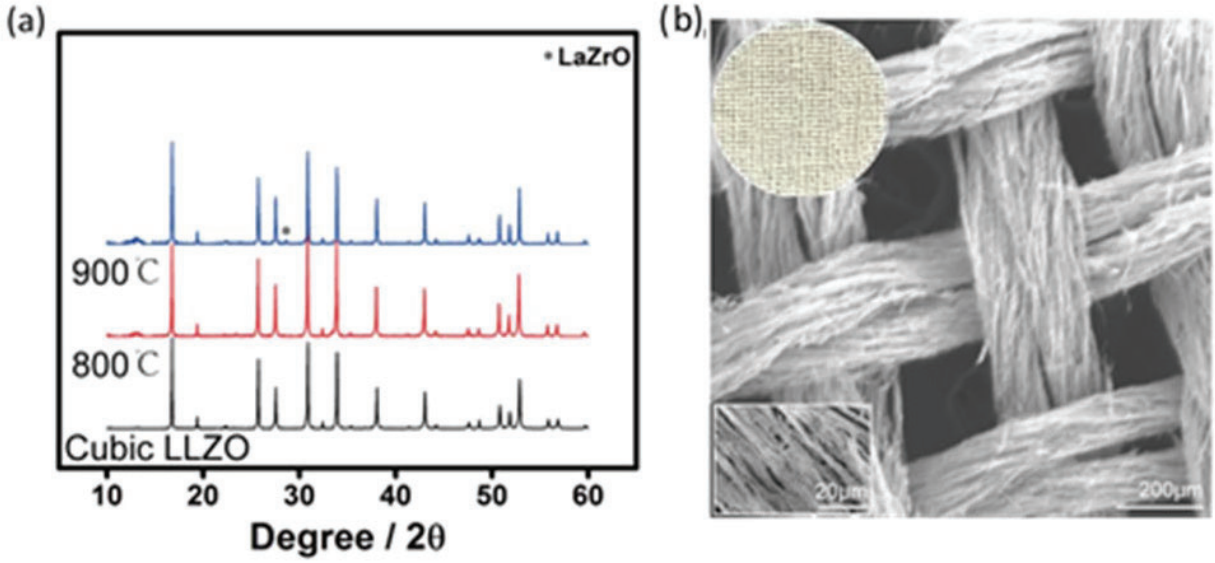

Figure 4. Characterization of garnet fibrous membrane: (a) Powder XRD patterns of the crushed garnet textile sintered at different temperatures; (b) SEM image of the garnet textile converted from the precursor solution impregnated template

1.3. Synthesis of lithium-ion conducting polymer

The polymer matrix was prepared by dissolving LiTFSI (Sigma Aldrich) and PEO (~600,000, Sigma Aldrich) in acetonitrile. Plasticizer was added to reduce the crystallinity and improve Li-ion conductivity at room temperature. The polymer electrolyte was cast on a Teflon block and dried in an argon-filled glove box, followed by drying in a vacuum oven to remove the residual solvent before electrochemical performance characterization. Electrochemical impedance of the polymer electrolyte was measured in a stainless steel/polymer/stainless steel configuration using a Solartron 1260 Impedance Analyzer. A Teflon spacer was included to fix the polymer thickness. Impedance tests were conducted with AC amplitude of 20 mV in the frequency range of 1 Hz and 1 MHz from 25 °C to 100 °C. Figure 5 presents the typical impedance plot for the polymer electrolyte measured at room temperature. Lithium-ion transfer processes were divided into ion conduction within the CPE (high frequency arc) and ion blocking at the CPE/stainless steel interface (low frequency inclined tail). The resistance of the CPE was obtained by reading the real impedance values at the high frequency intercept of the arc. Measured lithium-ion conductivities of the polymer electrolyte is 9×10^{-5} S/cm at 25 °C.

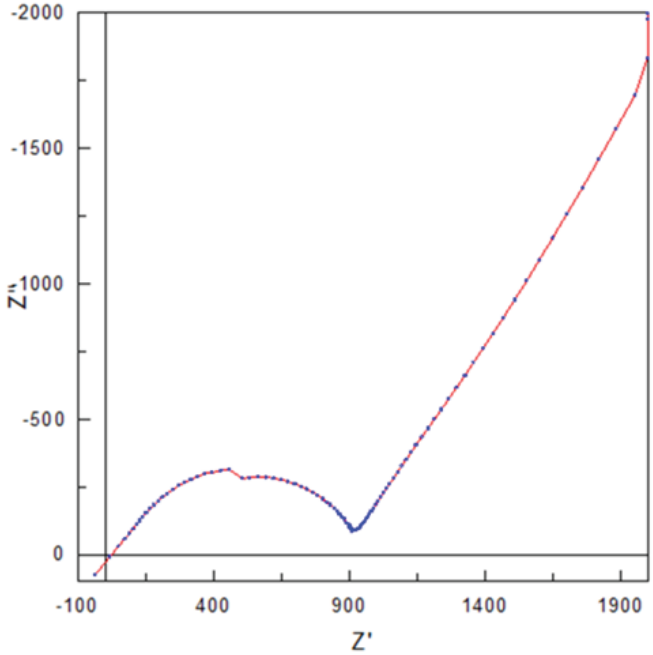

Figure 5. Impedance spectra of the polymer electrolyte at room temperatures. The Li-ion conductivity is 9×10^{-5} S/cm, calculated based on the dimension of tested sample.

1.4. Electrochemical, mechanical, and thermal properties of hybrid SSE

Hybrid composite polymer electrolyte was prepared by mixing the garnet fibers with polymer electrolyte in N-methyl-2-pyrrolidinone (NMP) in a glass beaker at 70 ºC using a magnetic stirrer. After 6 hours of stirring, the mixture was tape cast onto a Teflon block and left to dry at 80 ºC over-night. Figure 6 shows a photograph of the flexible hybrid composite polymer electrolyte and the AC impedance and CV of the composite polymer electrolyte. The room temperature Li^{+} conductivity is 6.07×10^{-4} S/cm and the electrochemical voltage stability window is over 4.5V.

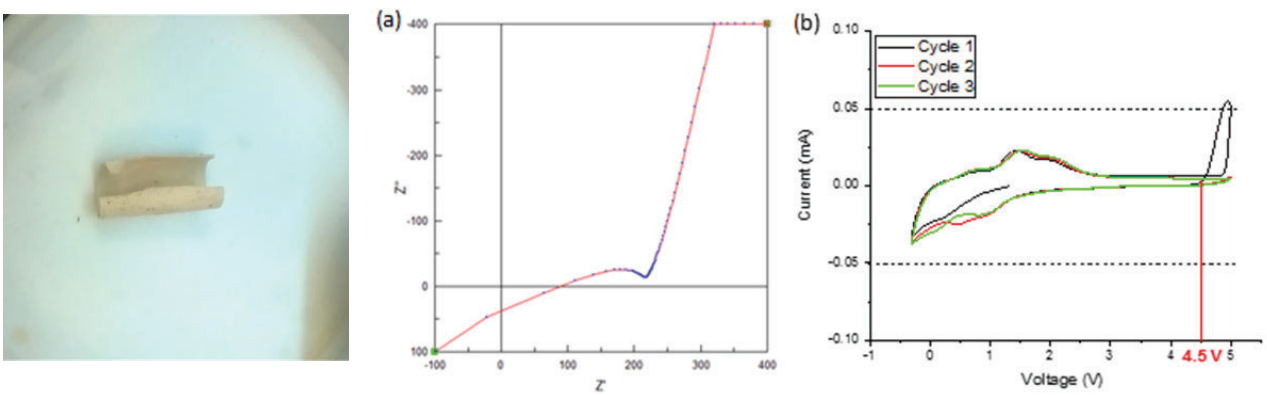

Figure 6. Photograph of the flexible hybrid composite polymer electrolyte; Electrochemical characterization of hybrid composite polymer electrolyte: (a) Ac impedance, Li-ion conductivity is 6.07×10^{-4} S/cm; (b) CV, stable up to 4.5V

Nanoindentation is a technique widely used for determining mechanical properties of the near-surface region of materials. By combining the application of low loads, measuring the resulting displacement, and determining the contact area between the tip of the indenter and the sample, hardness (H) and elastic modulus (E) are able to be measured. Nanoindentation was performed on a Hysitron Inc. TriboIndenter. The evaluated garnet fiber was soaked in melted crystal bond. The dried composite sample was mounted in slow-curing epoxy glue and polished. The optical microscope in the nanoindenter was used to select positions for indentation on the center of the fibers (Figure 7). The position of the center of the fiber was evaluated with individual scans of the AFM image and the location of the fiber was manually adjusted. Hardness and Young's modulus of garnet fiber was measured to be 0.28 ±0.04 GPa and 6.3±0.5 GPa, respectively.

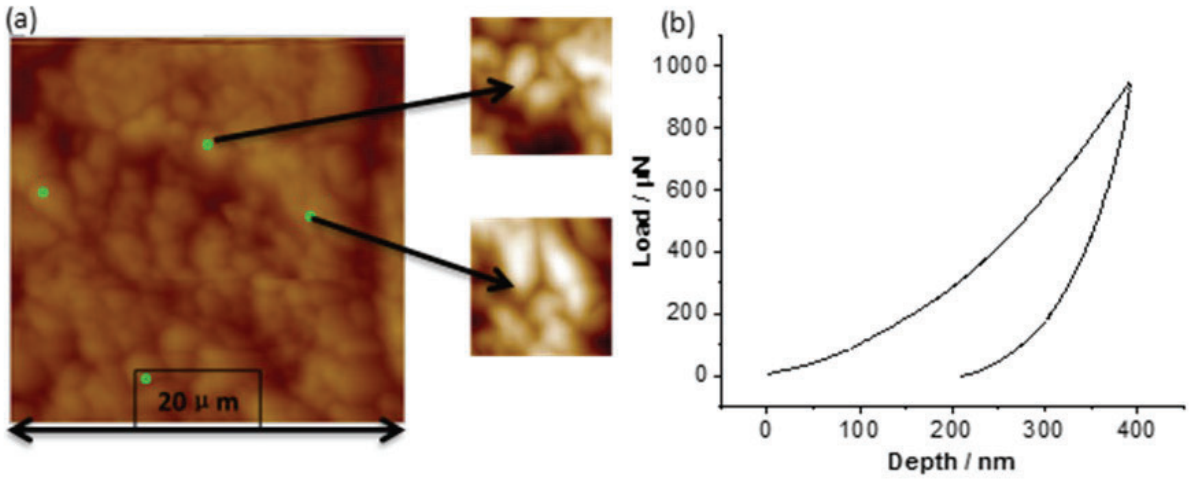

Figure 7. Mechanical characterization of garnet fiber: (a) AFM scanning of the nano-indent points on garnet fiber; (b) Load-depth profile of garnet fiber.

Hybrid SSE was developed and characterized using garnet nanofiber membranes. Al-doped LLZO with the chemical composition of $Li_{6.28}Al_{0.24}La_3Zr_2O_{11.98}$ was prepared. The cellulose nanofiber template was soaked in the garnet precursor solution and then treated at high temperature of 800 °C to obtain the ceramic membrane. The 3D structure of the garnet membrane was scanned using a LK-H082 semiconductor laser model. The reconstructed digital structure shows a typical over one-under one, plain weave textile pattern in Figure 8. Height of the membrane was indicated to be generally 200 μm by the cross-yarn junction areas in the pattern. The fiber structure was further analyzed by 3D FIB tomography in the Tescan XEIA FIB-SEM. The 3D sampling produced secondary electron images with good contrast between the ceramic fiber mat particles (which appeared bright) and the infiltrated epoxy (which appeared dark) in Figure 8. The continuous ceramic fiber provides structure reinforcement and abundant fast Li-ion conductive pathways within the composite electrolyte.

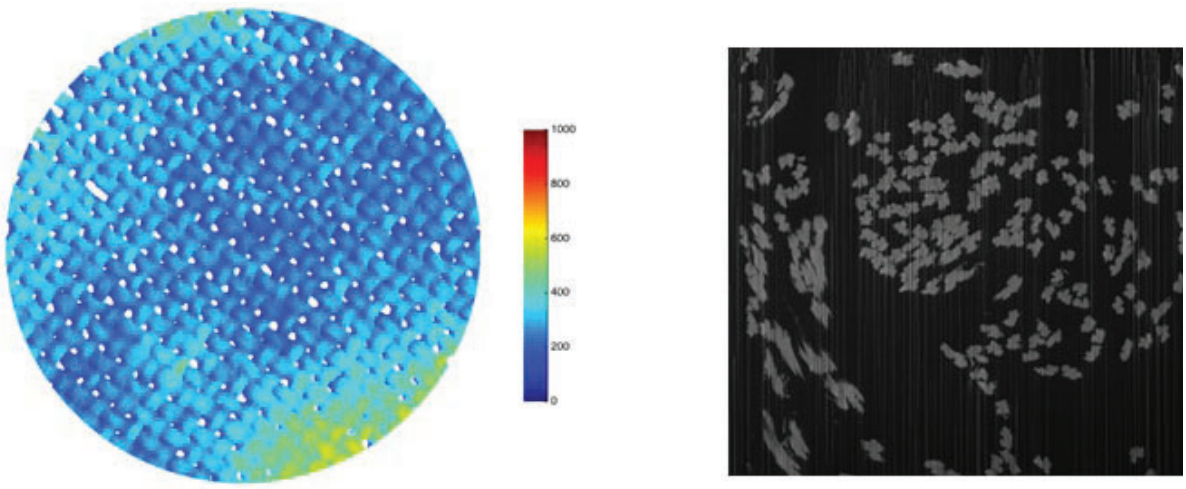

Figure 8. Characterization of garnet fibrous membrane: left, Reconstructed model of garnet nanofiber membrane flatness uniformity generated by 3D laser scanning; right, Focus ion beam analysis of the typical fiber bundle structure in garnet membrane.

Hybrid electrolyte was fabricated by infiltrating conductive polymer into the multi-level open space in the garnet fiber membrane. Surface morphology of the hybrid electrolyte was analyzed by AFM within an area of 10 μm×10 μm in Figure 9. The polymer material fully filled the open pores and covered the surface of the individual fibers. The surface roughness of the hybrid electrolyte was effectively limited to a value of less than 2 μm. Thermal performance of the hybrid electrolyte was analyzed by thermogravimetry measurement. The weight loss is caused by evaporation of the trapped solvent from room temperature to 300 °C. The hybrid electrolyte shows thermal stability up to 450 °C.

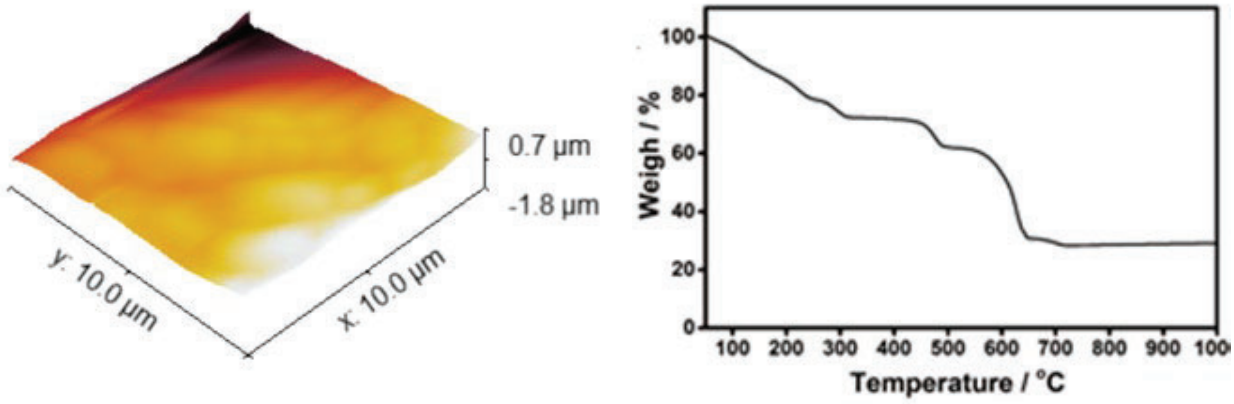

Figure 9. Characterization of hybrid electrolyte membrane: left, AFM scanning of the hybrid electrolyte membrane; right, Thermal properties of the hybrid electrolyte membrane.

1.5. Fabrication of thin hybrid electrolyte

We developed a nanofiber template membrane to further reduce the thickness of the hybrid

electrolyte. PAN (Polyacrylonitrile) fiber membrane was electrospinned and hot pressed as the sacrificial template. Figure 10 shows the photo images of the PAN fiber template. The as-prepared PAN fiber mat by electrospinning was 81 µm thick on the left. To reduce the thickness and retain the fiber structure, hot press was applied and the final thickness of 15 µm can be achieved after pressing at 180 °F for 30 min. The pressed template was stabilized in air at 260 °C for 10 h was used for garnet precursor infiltration.

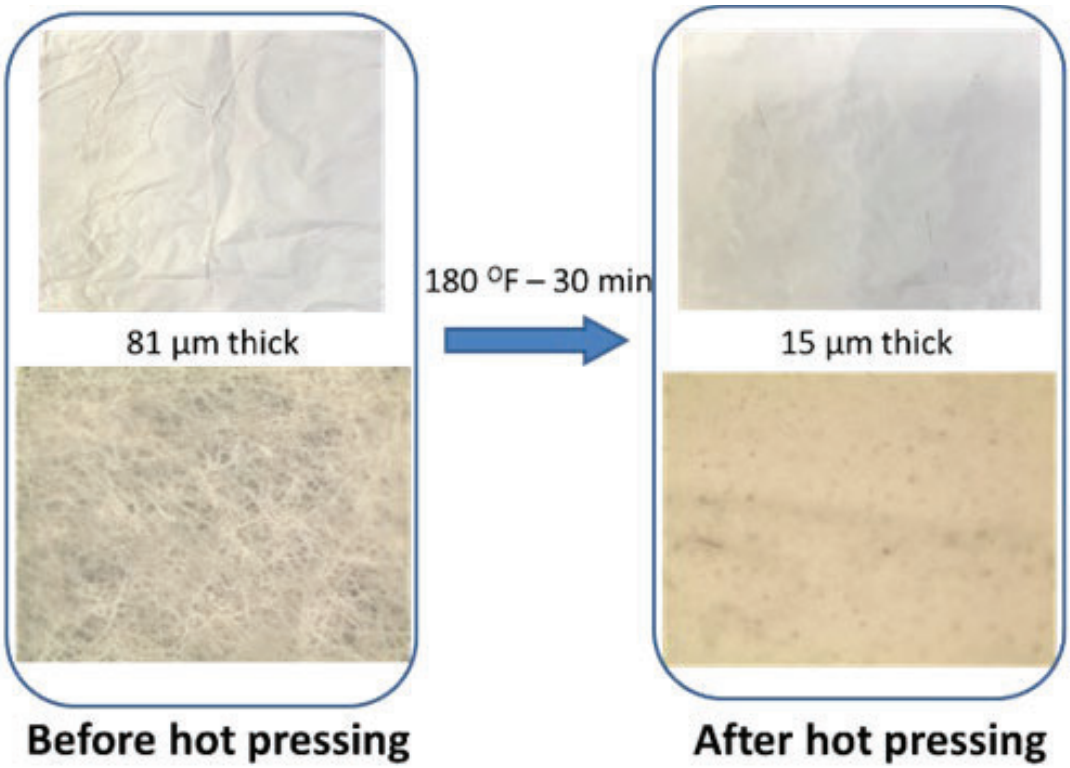

Figure 10. Fabrication of 20 µm electrospinning fiber mat as template for garnet precursor infiltration. Left: as-prepared fiber mat by electrospinning; right: mat hot pressed at 180 °F for 30 min.

The soaked membrane was sintered at 800 °C in oxygen. Figure 11 shows the SEM images of the sintered garnet nanofiber membrane. Thickness of the gannet nanofiber membrane is less than 30 µm with a typical layered structure. The thin garnet fiber framework was used for conductive polymer infiltration to make hybrid electrolyte.

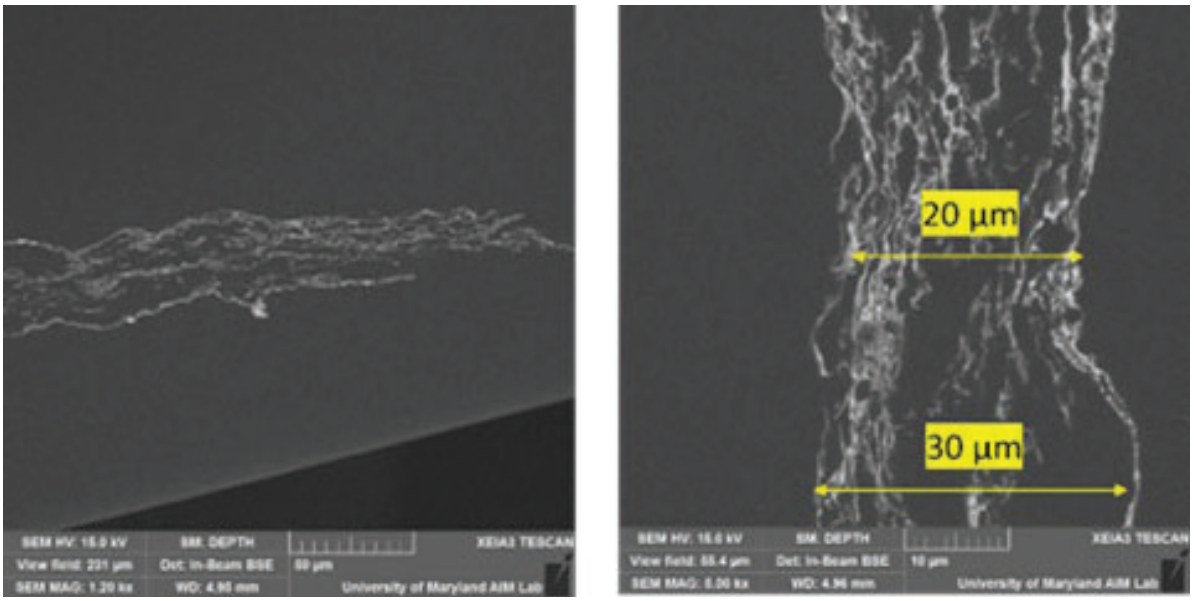

Figure 11. Sintered garnet precursor infiltrated fiber mat template. Sample was impregnated with epoxy for SEM analysis.

Li-ion conducting polymer was infiltrated into the porous garnet nanofiber membrane to make hybrid electrolyte. The as-infiltrated electrolyte was hot pressed to further reduce the thickness and a hybrid electrolyte as thin as 11 microns was achieved, as shown in Figure 12. The hybrid electrolyte appears to be homogenous, dense and flexible.

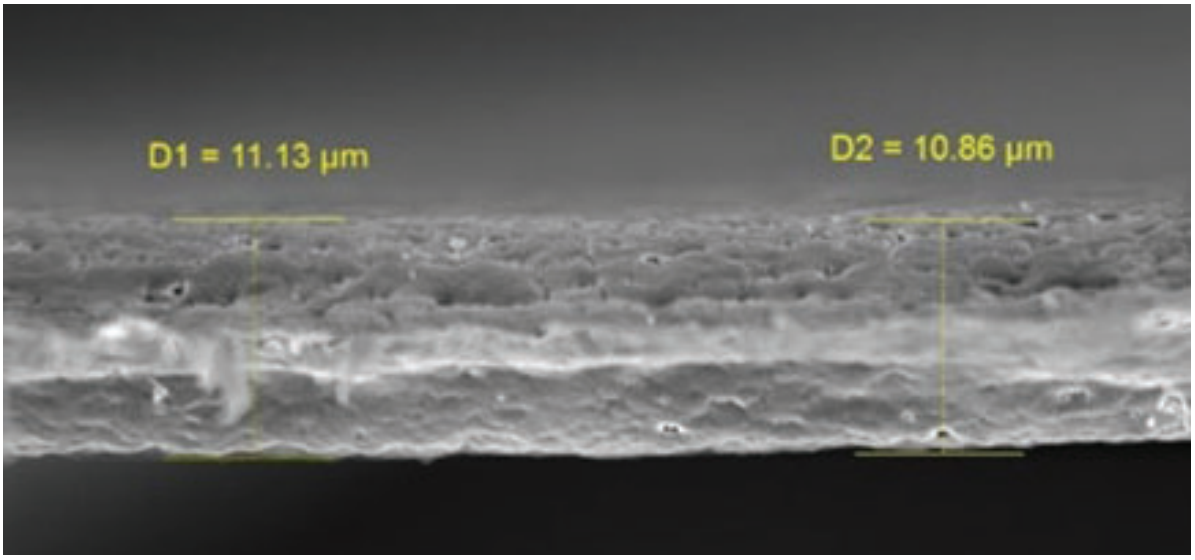

Figure 12. Hybrid electrolyte membrane with the thickness ~11 µm

2. Li Cycling of Hybrid Electrolyte

2.1. Understanding lithium cycling in thin SSE at current density of 3 mA/cm^2.

Using the thin hybrid electrolyte and lithium metal, we assembled symmetrical cells for electrochemical characterization. The symmetrical cells were fabricated by pressing two pieces of lithium metal on both sides of the electrolyte by hydraulic crimping. The cell was tested using Solatron 1260 and 1287 stations. The initial impedance of the cell was measured from 10^7 to 10 Hz with an AC amplitude of 100 mV at room temperature. Two arcs are observed for the cell as shown in Figure 13. The first suppressed arc at high frequency range is from the resistance of electrolyte. The second arc at low frequency range originated from the interface between lithium metal and electrolyte. Thus, the interface resistance is higher than that from the electrolyte due to the impurity phase on the surface of lithium metal. The electrochemical performance of the symmetric cell was further evaluated by stripping and plating using an Arbin electrochemical testing station at room temperature. Figure 13 shows the preliminary cycling results. The voltage profiles of the cell show stable performance at different current densities of 0.1 mA/cm^2 and 0.5 mA/cm^2. The resistance calculated from the cycling matched well with the AC impedance. The Li plating/stripping performance was tested up to 3 mA/cm^2. The symmetric Li/electrolyte/Li cell shows overpotential around 1 V without shorting.

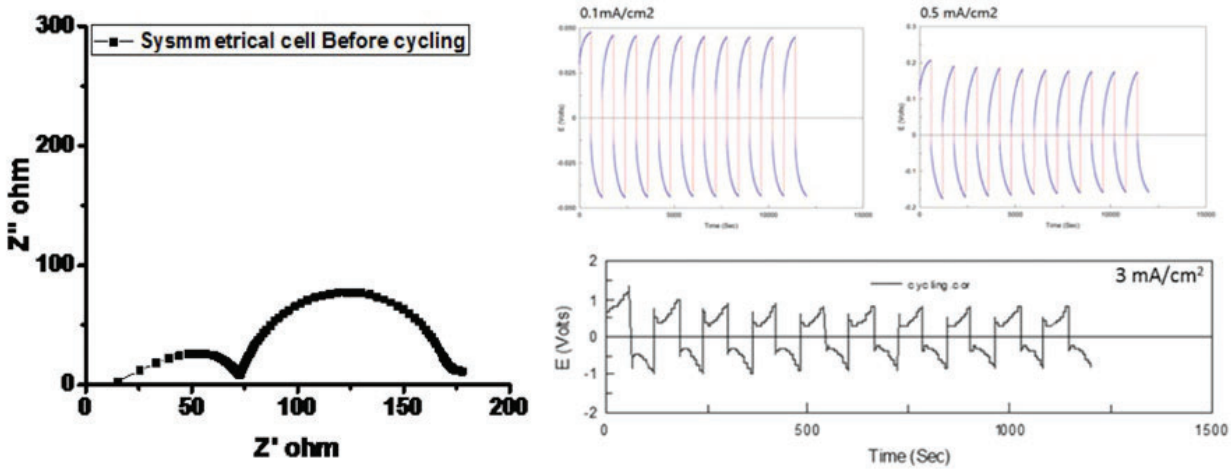

Figure 13. Electrochemical impedance of the Li/electrolyte/Li symmetric cell at room temperature (left); Cycling of the cell at different current densities of 0.1 mA/cm^2, 0.5 mA/cm^2 and 3 mA/cm^2

Figure 14 shows voltage profiles of the cycling cell at different current densities of 0.1 mA/cm^2 and 3 mA/cm^2. The cell was initially cycled under low current density to stabilize the lithium metal/hybrid electrolyte interfaces. The cell shows stable and uniform lithium stripping/plating behavior with flat cycling plateaus. After stabilization, the cell was cycled at high current density of 3 mA/cm^2 for 500 cycles. As current density was increased by 30 times, overpotential of the cell increased. The cell was successfully cycled at 3 mA/cm^2 for 500 cycles without dendrite penetrating through the hybrid electrolyte.

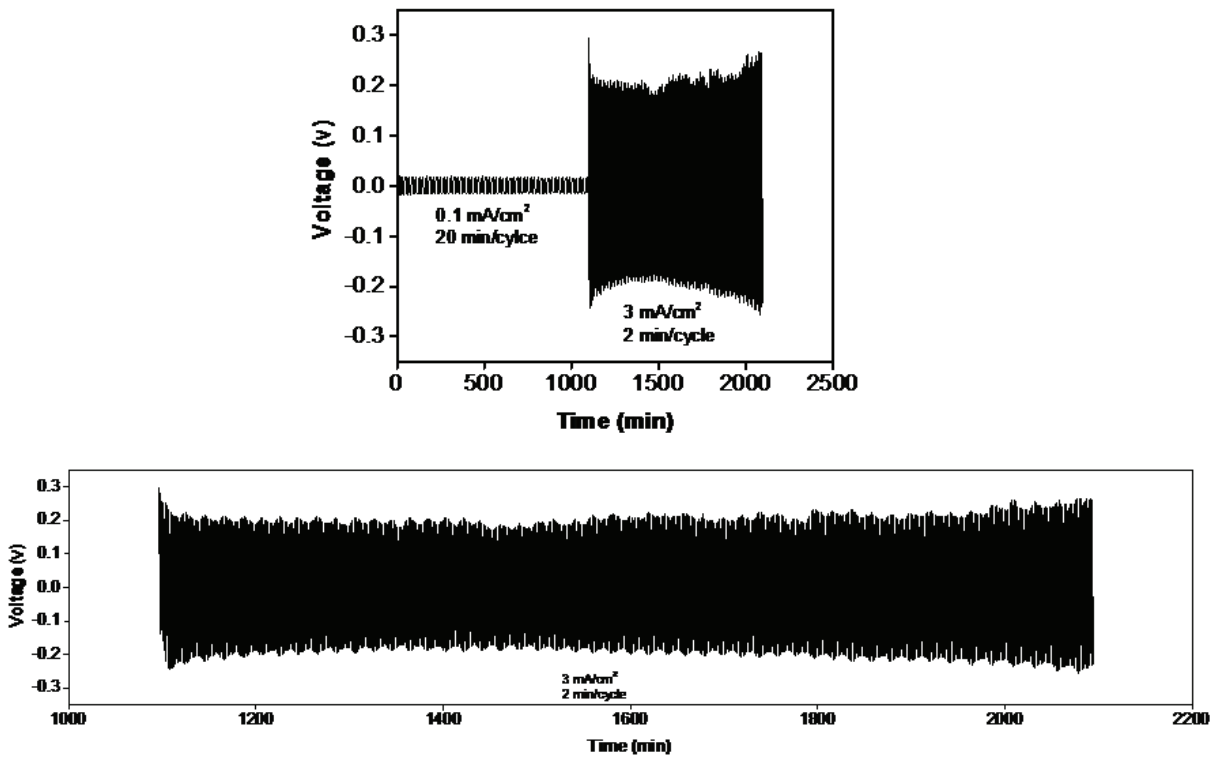

Figure 14. Electrochemical cycling of the Li/electrolyte/Li symmetrical cell, including low current density stabilization at 0.1 mA/cm^2 and high current density cycling at 3 mA/cm^2 (top); enlarged plot at 3 mA/cm^2 for 500 cycles without lithium dendrite penetration (bottom).

3. Computational Analysis of Conductivity, Mechanical Properties, and Dendrite

3.1. Li ionic diffusion in garnet nanofibers and its response to mechanical deformation.

In order to perform molecular dynamics (MD) simulations for garnet nanofibers, we implemented and tested force fields for lithium garnet $Li_7La_3Zr_2O_{12}$ (LLZO). Using the newly tested force field, the lattice parameters in tetragonal and cubic phases of LLZO were calculated using MD simulations as a function of temperature, in good agreement with experimental values. Li^+ diffusion in LLZO were also modeled using MD simulations. The calculated Li^+ conductivity and activation energy of LLZO are in good agreement with *ab initio* calculations and experimental measured values.

Atomistic model of garnet nanofibers was constructed and equilibrated in MD simulations (Figure 15). The Li^+ transport in single garnet nanofiber was modeled using MD simulations at different temperatures. The Li^+ conductivities at different temperatures and the activation energies for Li^+ diffusion was calculated in single garnet nanofibers. The Li^+ diffusion properties from MD simulations were compared to the bulk phase of LLZO and show faster Li^+ diffusion in single garnet nanofibers than in bulk garnet. In addition, Li^+ migration mechanism was analyzed for Li^+ transport along and perpendicular to the nanofiber direction, and at surface and core regions of the nanofiber. Insight into Li^+ diffusion in garnet nanofiber was obtained.

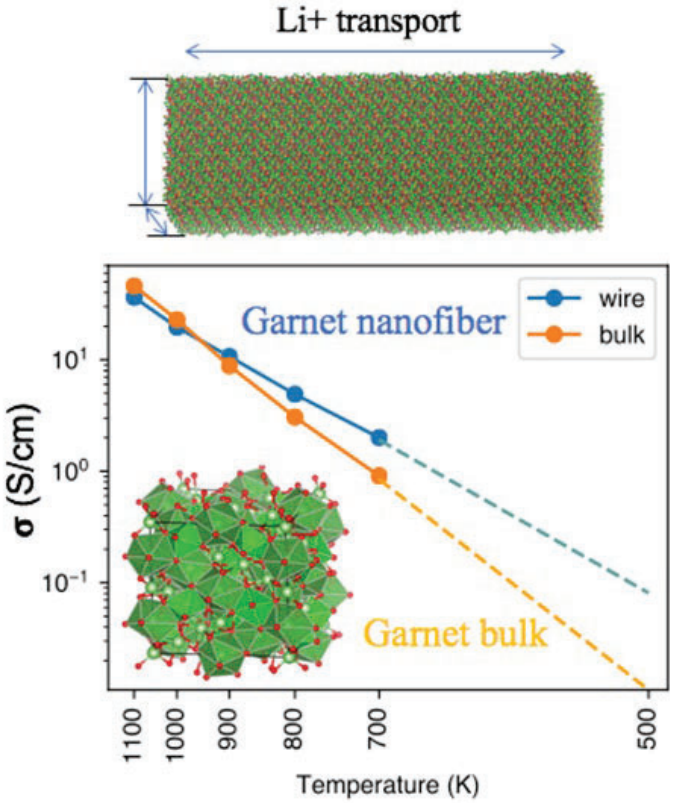

Figure 15. Computer modeling of Li^+ transport in garnet nanofibers.

Mechanical deformation on garnet bulk and nanofiber was performed under MD simulations. The elastic modulus from our calculations are in good agreements with experiments. The Li^+ diffusion under mechanical deformation was studied using MD simulations (Figure 16). We simulated the garnet at both tensile and compressive stress with different strain (1% and 3%). We found the mechanical deformation significantly impacts in Li^+ diffusion. Li conductivity decreases and activation energy increases in both stressed states. This change is in good agreement with experiments. The MD simulations in both bulk and nanofiber show similar results. Mechanical deformation decreases Li^+ conductivity in garnet. Both tensile and compressive deformation drives garnet towards slow-conducting tetragonal phase. In summary, MD simulations were performed to understand Li^+ diffusion in garnet nanofibers and the effect of mechanical deformation.

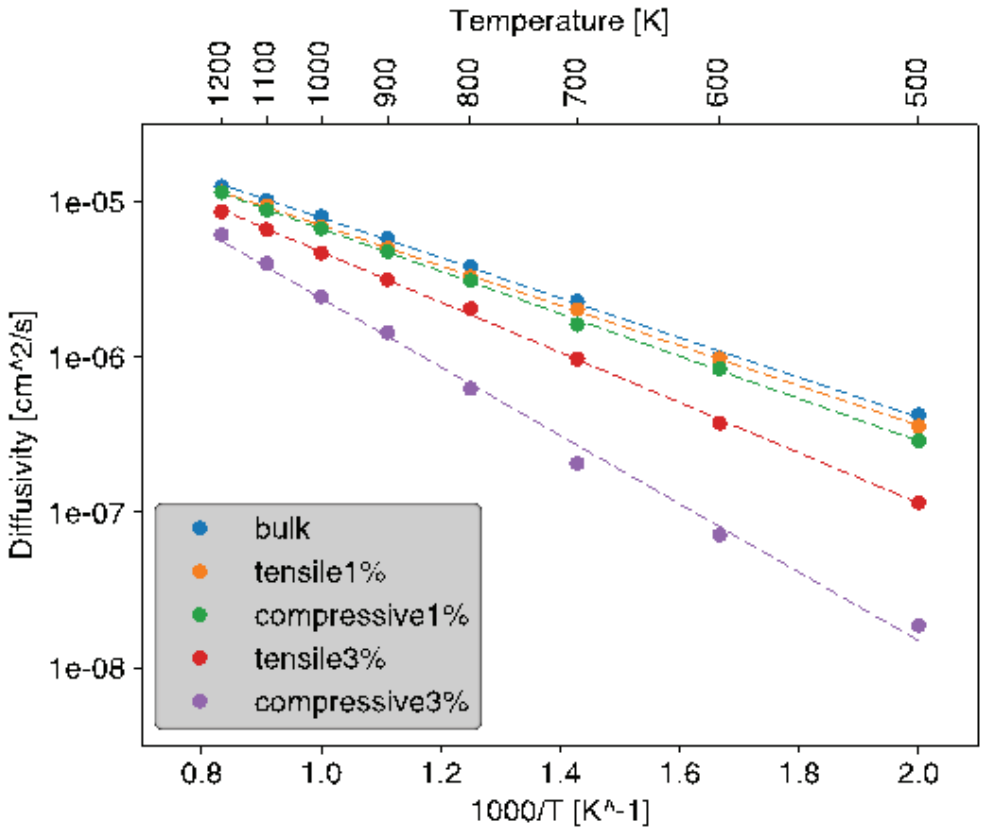

Figure 16. Li diffusion of garnet under strain.

3.2. Understanding lithium cycling in thin SSE at current density of 3 mA/cm^2.

Computational modeling was performed to evaluate various fundamental processes that are related to the Li dendrite growth in SSEs, including defect chemistry and energetics, Li-ion diffusion in nanofibers and grain boundary, and local potential distribution. We performed DFT calculations on the formation of various point defects in garnet (Figure 17), which may significantly impact the Li dendrite growth mechanism within garnet solid electrolyte. Our calculation found Li^+ insertion into garnet may be energetically favorable in contact with Li metal, in agreement with experimental observations. The calculations also found oxygen vacancy formation may be favorable at Li rich conditions, which may aid Li metal reduction and dendrite formation. The formation and transport of electron polarons is also evaluated in DFT calculations, which was speculated to contribute to Li reduction inside garnet SSE. In order to understand Li dendrite growth mechanism within garnet solid electrolyte, MD simulations were performed on garnet grain boundaries (Figure 17). We observed the decrease of Li^+ diffusion near the grain boundary core, causing by distortion of garnet crystal structural framework near the grain boundary core. Grain boundaries may cause significant potential drop or field concentration, and may aid Li nucleation and Li dendrite growth, as shown by continuum modeling (Figure 17).

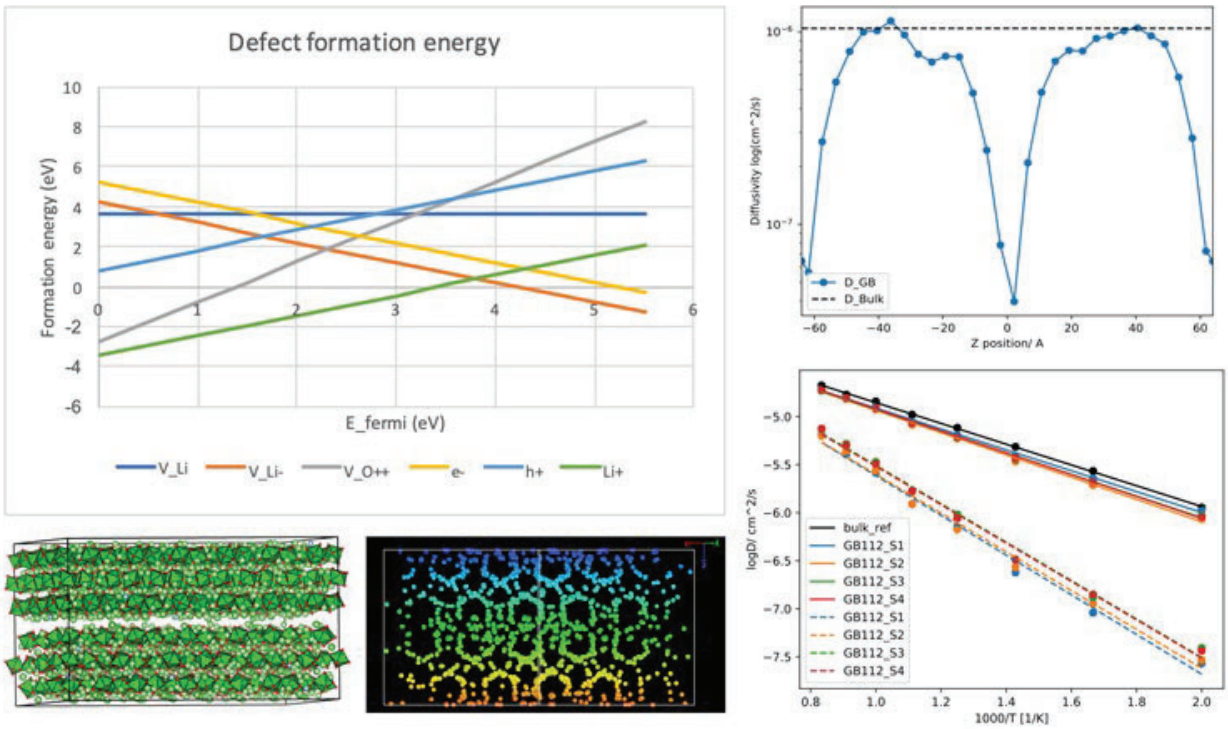

Figure 17. Formation energy of point defects in LLZO (left) and Li ion diffusion in LLZO grain boundary (right) from atomistic modeling.

Computer modeling was performed for the Li nucleation and Li dendrite growth within the SSE. We modeled the electronic potential and ionic transport within the SSE with different microstructural features during Li cycling. For the SSE with Li dendrite formed inside, the modeling results (Figure. 18) shows high ion current density near the tip of Li dendrite, indicate the increase of Li chemical potential and the driving force for Li dendrite growth. We also found that similar behavior exists in the intersection of grain boundaries in SSE, which are caused by the slow ionic diffusion and high resistances in the grain boundaries. This behavior also suggests the favorable Li dendrite growth in grain boundaries of SSEs, consistent with numerous reports in the literature. We found that in the hybrid SSEs these hot spots for Li dendrite growth do not exist because of the well-connected fast-ion conducting of garnet fibers formed inside the hybrid SSE. This modeling result is consistent with the high current density 3 mA/cm^2 cycling observed in the Li cycling experiments of hybrid garnet SSEs.

Figure 18. Heat map of Li dendrite formation in SSE with various microstructural features.

3.3. Modeling of lithium dendrite protection

Computational modeling is performed to evaluate various fundamental mechanisms that are related to the Li dendrite growth and protections in SSEs. The Li metal dendrite nucleation and growth as a function of garnet interface morphology and microstructures are evaluated using first principles computation and continuum modeling (Figure 19). First principles calculations were performed to evaluate the surface energy of garnet and the interface energy between Li metal and garnet surfaces. These elementary energies of surfaces and interfaces were used to model the energetics of lithium deposition into garnet void. Using nucleation theory models, the energy barrier and critical nucleation size of Li metal growth within the garnet pores or inside the garnet were evaluated and compared. The critical nucleation barrier is greatly affected by the applied overpotential, and the critical radius is as small as a few Å at large over potential, suggesting easy Li metal nucleation at large over potential. These results are consistent with numerous experimental reports of Li metal plating in solid electrolyte. The results also found that the filling of Li metal inside the pores are energetically more favorable than growth into garnet crystals. This result suggests that having a porous structure of garnet promotes Li metal growth within the pores preferentially, in agreement with our experimental observations.

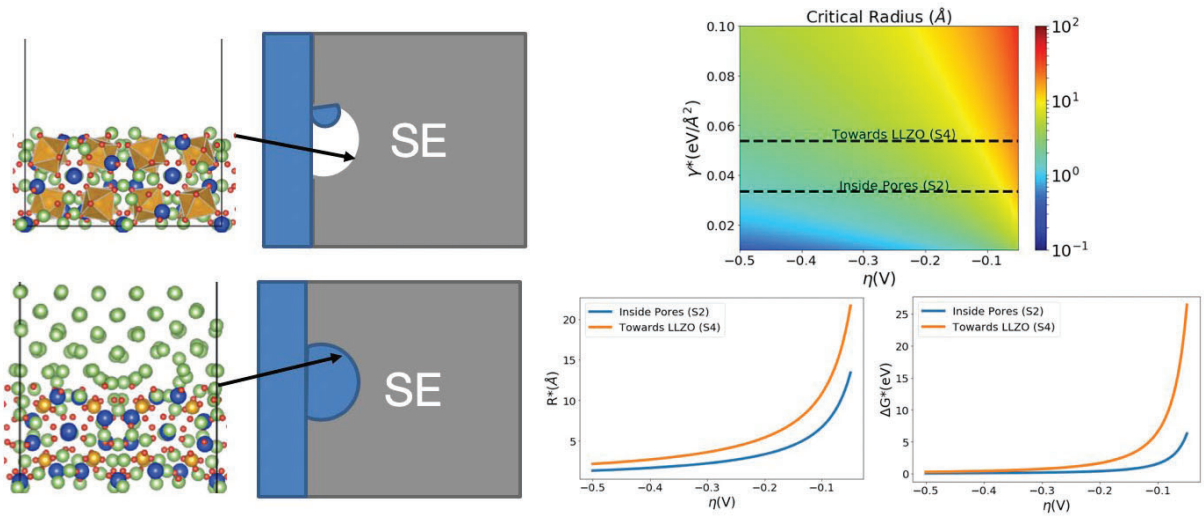

Figure 19. Ab initio models of garnet surface and Li-garnet interface (left); the schematics of lithium growth inside garnet pores or garnet (middle); the critical nucleation energy and the critical nucleus radius (right).

In order to study Li nucleation and dendrite growth, we modeled the electronic potential and ionic transport within the SSE with different microstructure features at applied potentials. The modeling results (Figure 20) show high ion current density near the tip of Li dendrite, indicating an increase of Li chemical potential and the driving force for Li dendrite growth. The Li dendrite growth in hybrid SSEs is greatly mitigated by the well-connected fast-ion conducting garnet fibers formed inside the hybrid SSE, as this modeling result shows smaller hot spot and driving force for Li metal nucleation. For Li-garnet interfaces, we studied the Li current distribution of the poorly contacted Li-garnet interface, which may happen for non-treated garnet surfaces. In this case, we found the non-contacting interface lead to concentrated lithium current spot, suggesting stronger tendency for Li dendrite formation in agreement with experiments. Therefore, maintaining a good interface contact is crucial for reducing Li current concentrations and mitigating Li dendrite formation. The effect of interfacial coating layers, which are demonstrated to protect interface, on the surface was also studied. It was found coating layers can help mitigate the current density hot spot, leading to protecting of the interface. In addition, the effect of conductivity of coating layers was studied and revealed.

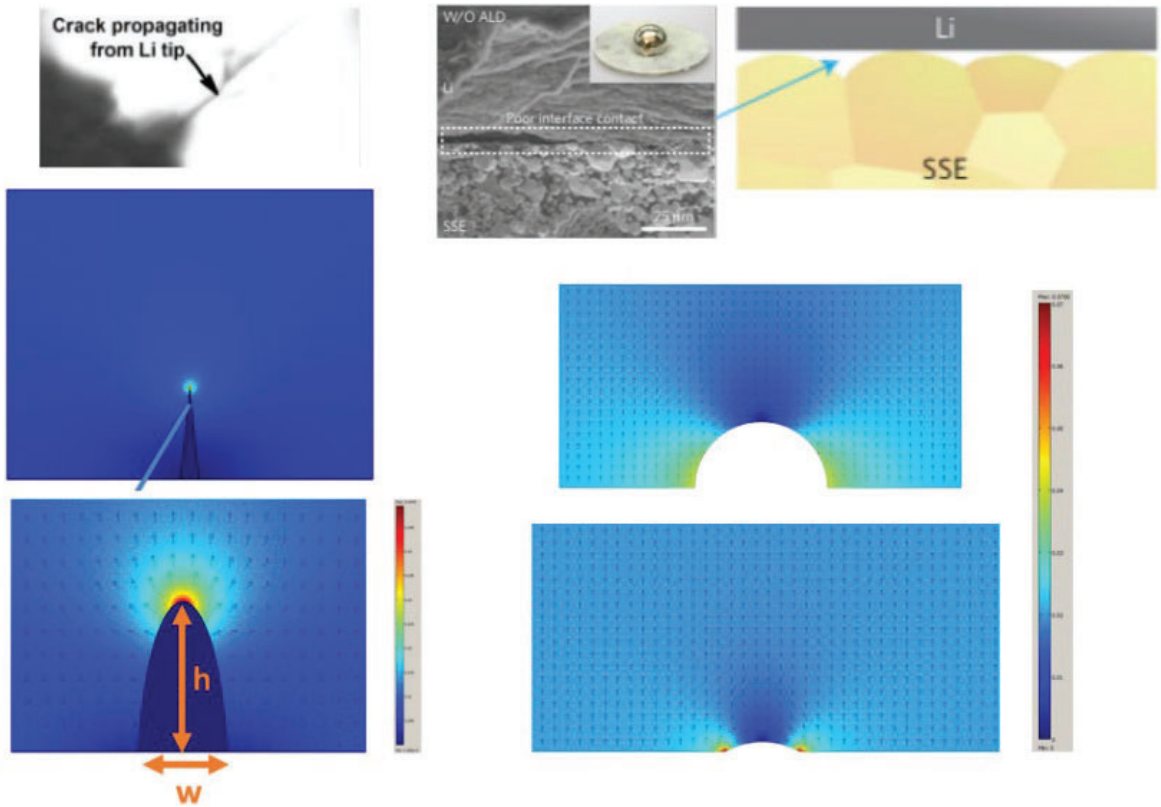

Figure 20. The current concentration in Li dendrite tip in garnet (left) and in a poorly contact Li-garnet interfaces.

4. Hybrid Electrolyte Li-S Full Cell Performance

4.1. Fabricate porous mixed electron/ion conductor

Porous ion-conducting frameworks composed of garnet ceramic fibers was fabricated by a sacrificial template method as described above. Carbon nanotube solution (1 mg/ml in NMP) was infiltrated into the pore structure and overcoated the exposed surface of the garnet phase. Therefore, mixed electron/ion conductor was achieved in Figure 21 (a). The gray composite conductor provides both ion and electron conduction by sintered garnet electrolyte and carbon nanotube layer, respectively. The ionic conductivity was measured by Solartron 1260 impedance analyzer. The AC impedance plot shows a typical compressed semi-circle in high frequency range in Figure 21 (b), representing the ion conduction process occurred along the interconnected fibrous garnet phase. The electronic conductivity was measured by Keithley 2400 source meter, as shown in Figure 21 (c). The linear relationship between the applied voltage and the resulting electric current obeys the Ohm's law, indicating that the conformal carbon nanotube coating layer has created an electronic conduction network.

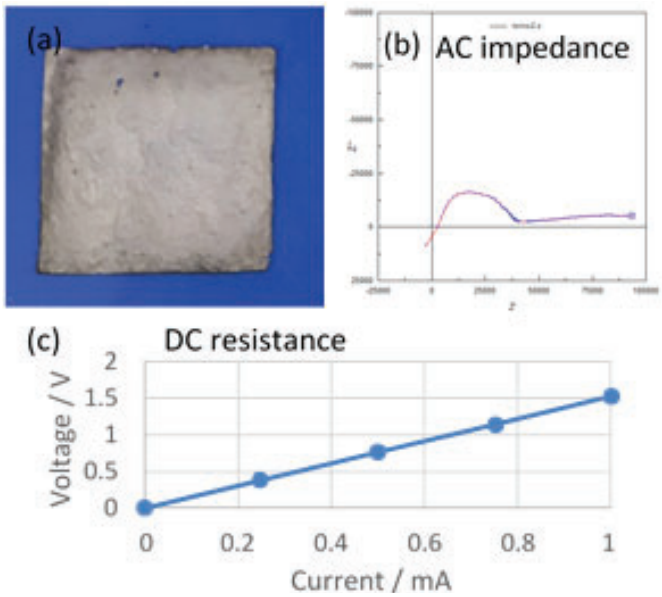

Figure 21. Porous mixed electron/ion conductor and the electrochemical performance: (a) photo image; (b) AC impedance plot; (c) DC resistance plot.

Lithium polysulfide solution (1 mol/L Li_2S_8 in DOL/DME) was synthesized for sulfur cathode fabrication. The solution was infiltrated into the pore structure of the mixed electron/ion framework to achieve desired sulfur loading. The microstructure of sulfur infiltrated mixed conductor was studied by SEM in Figure 22. Deposition of carbon nanotubes and lithium polysulfide reconstructed the surface of garnet fiber to generate well-bonded garnet/carbon/sulfur three-phase microstructure. The elemental mapping confirmed the existence of garnet phase, carbon phase and polysulfide phase, indicating successful infiltration of carbon nanotubes and polysulfide into the porous garnet fiber framework.

The fibrous garnet structure, together with the carbon nanotubes coating layer formed a continuous network of pathways for both ion and electron transport, which successfully built the backbone for a three-dimensional solid-state high-loading sulfur cathode.

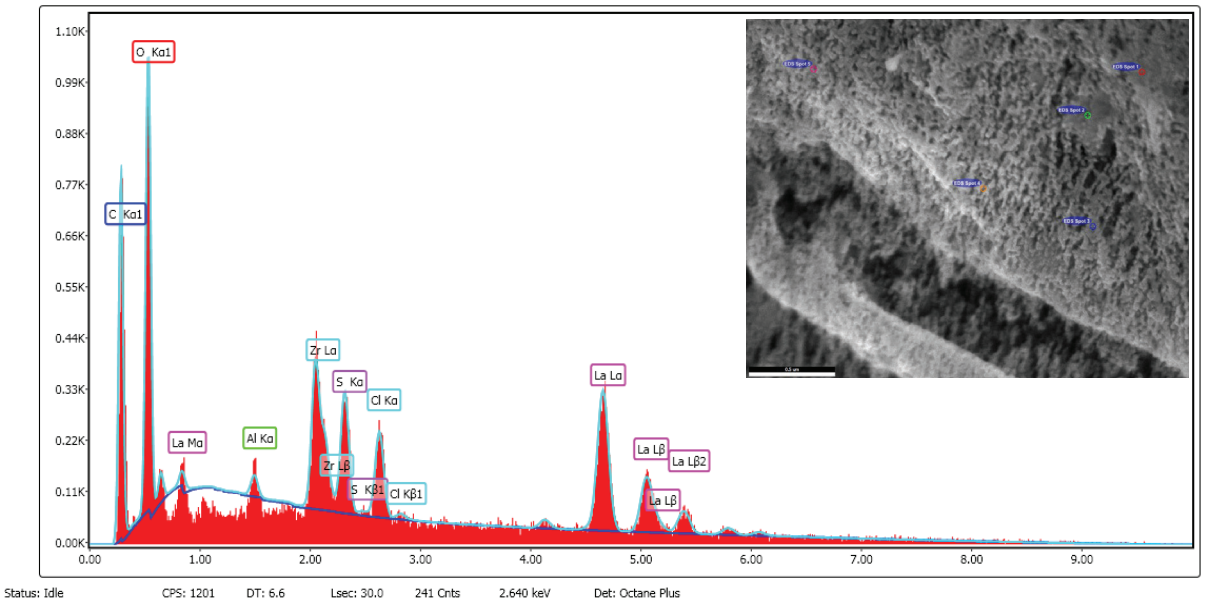

Figure 22. Sulfur cathode infiltrated porous mixed electron/ion conductor

4.2. Li-S Full cell performance

Two sulfur-cathode approaches were investigated to obtain high areal capacity of sulfur for full cell fabrication with the hybrid SSE electrolyte. For the first a 3D host material aligned microchannels was used for loading sulfur with high mass loading. As schematically shown in Figure 23a, a piece of carbon with perpendicular channels were carbonized (c-wood) and filled with graphene. S was then melted and infiltrated into the pores of the c-wood/graphene host material with a mass loading of ~20 mg/cm^2. The electrochemical performance of the high-loading S cathode (S@c-wood/graphene) was first demonstrated in liquid electrolyte, 1 M LiTFSI dissolved in DOL/DME and the discharge/charge voltage profile is shown in Figure 23b. The S@c-wood/graphene shows a high discharge capacity at 0.01 C and extremely high areal capacity. In the first discharge, the areal capacity is ~14 mAh/cm^2, which can be used with the flexible hybrid solid electrolyte for high-capacity Li-SSE-S full cells.

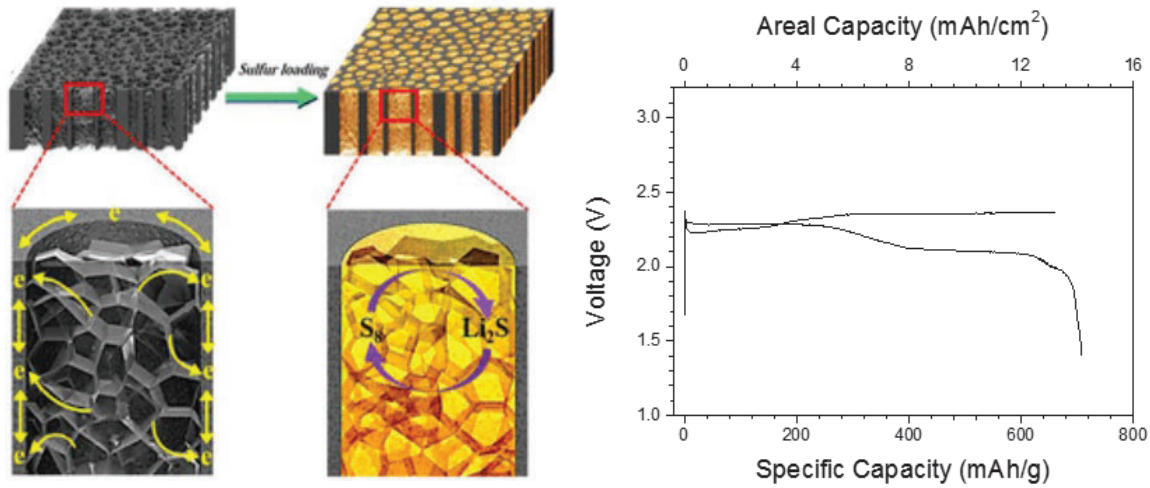

Figure 23. (a) Schematic of the preparation and the structure of the high-loading S cathode in c-wood with graphene. (b) First discharge/charge voltage profile of the S@c-wood/graphene

For the second approach a cathode was prepared by adding 1 M Li_2S_8 catholyte into a conductive carbon substrate with area of 1.27 cm^2. The polysulfide catholyte was prepared by mixing stoichiometric amounts of sulfur and Li_2S in a 1,3-dioxolane (DOL) and 1,2-dimethoxyethane (DME) solution (50:50 vol) with 1 M lithium bis(trifluoromethanesulfonyl)imide and 2 wt.% lithium nitrates. The mixed precursor solution was stirred at 70 °C for 12h in a glove box. For full cell assembly, thick lithium metal foil was used as the anode. Electrochemical testing was carried out and analyzed with a battery cycler (Arbin Instruments) in the voltage window of 2.8–1.8 V at current density of 0.1 mA/cm^2. Electrochemical testing of the full cell was carried out with standard CR2032 cell using 175 µm-thick lithium metal counter electrode. Four pieces of stainless-steel spacers (0.2 mm thick) were used to achieve good contact between the electrolyte and electrodes. The electrochemical performance of the lithium-sulfur cell was analyzed with a battery cycler (Arbin Instruments) in the voltage window of 1.5–3.0 V at 0.1 mA/cm^2. Figure 24 shows the voltage profiles of the full lithium-sulfur cell. The discharge curve shows one sloping plateau around 2 V, which represented a solid-state type conversion of Li_2S_8 to Li_2S. The charging curve shows only one plateau, which is often seen in the most common electrolyte based on 1:1 vol DOL and DME. The hybrid electrolyte prevented polysulfide anion diffusion and thus avoided the shuttle effect issues.

The discharge plot of the lithium-sulfur battery in Figure 25 shows two plateaus at 2.3 V and 2.1 V. The lithium-sulfur battery generated a total capacity of 12.5 mAh, which meets the milestone of achieving 10 mAh full cell. Energy densities of the lithium-sulfur battery are calculated based on weight or volume of the cell components in Table 1 (spacers, spring and coin cell case are not considered for energy density calculation).

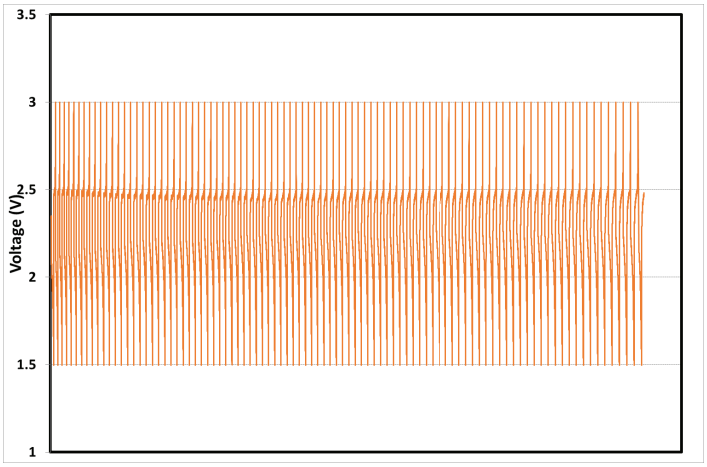

Figure 24. Charge-discharge profiles of Lithium/sulfur cell using hybrid electrolyte at 0.1 mA/cm^2.

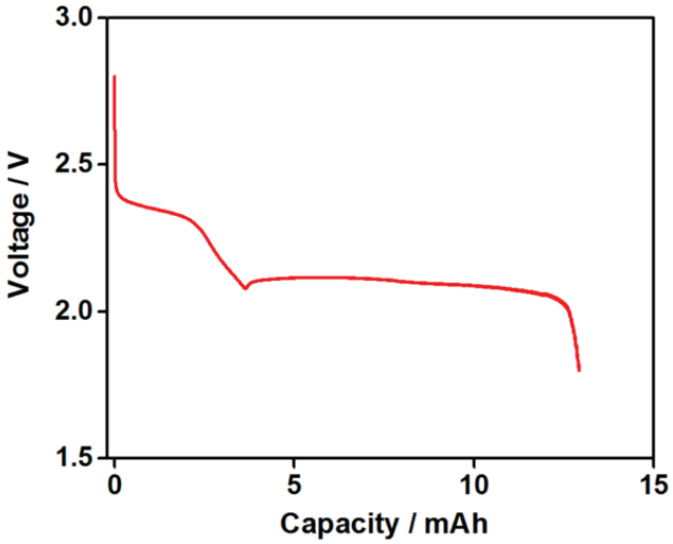

Figure 25. Discharge profile of a high capacity lithium-sulfur cell using hybrid electrolyte at 0.1 mA/cm^2.

Table 1 Energy density of the lithium-sulfur battery

	Lithium foil	Hybrid electrolyte	Carbon substrate	Li_2S_8 catholyte	Energy density
Weight/g	0.0118	0.0093	0.027	0.1105	195 Wh/kg
Volume/cm^3	0.0222	0.004	0.0076	0	776 wh/L

(1) Lithium metal anode: area, 1.27 cm^2; thickness, 175 µm; density, 0.534 g /cm^3.
(2) Hybrid electrolyte: area, 1.98 cm^2; thickness, 20 µm; density of garnet, 5.08 g /cm^3; density of polymer matrix, 1.2 g/ cm3; porosity of garnet framework, 70%.
(3) Conductive carbon substrate: area, 1.27 cm^2; thickness, 60 µm; density, 2.1 mg/cm^2.
(4) Catholyte solution: volume: 80 µl; 1 M LiTFSI; 0.5 M Li_2S_8; DOL/DME 50/50 vol.

Figure 26 shows the electrochemical performance of another hybrid SSEW electrolyte cell using a lower capacity sulfur cathode for 300 cycles. We found that the capacity continuously increased for the first 100 cycles, which is distinct from the tendency of Li-S batteries to lose capacity over time. It is observed that capacity doubled after 100 cycles. Thereafter, the cell gave high reversible discharge/charge capacities in the following cycles with efficiency above 98%, exhibiting good electrochemical performance over 100 cycles. The capacity started to fade slowly after 100 cycles. The battery maintained 95 % of capacity after 300 cycles. Due to the irreversibility of the side reactions, Coulombic efficiency over 100% was attained in the initial 40 cycles. Thereafter, the battery showed high reversible cycling capacities in the following cycles with a coulombic efficiency above 98%, exhibiting good electrochemical stability over 300 cycles.

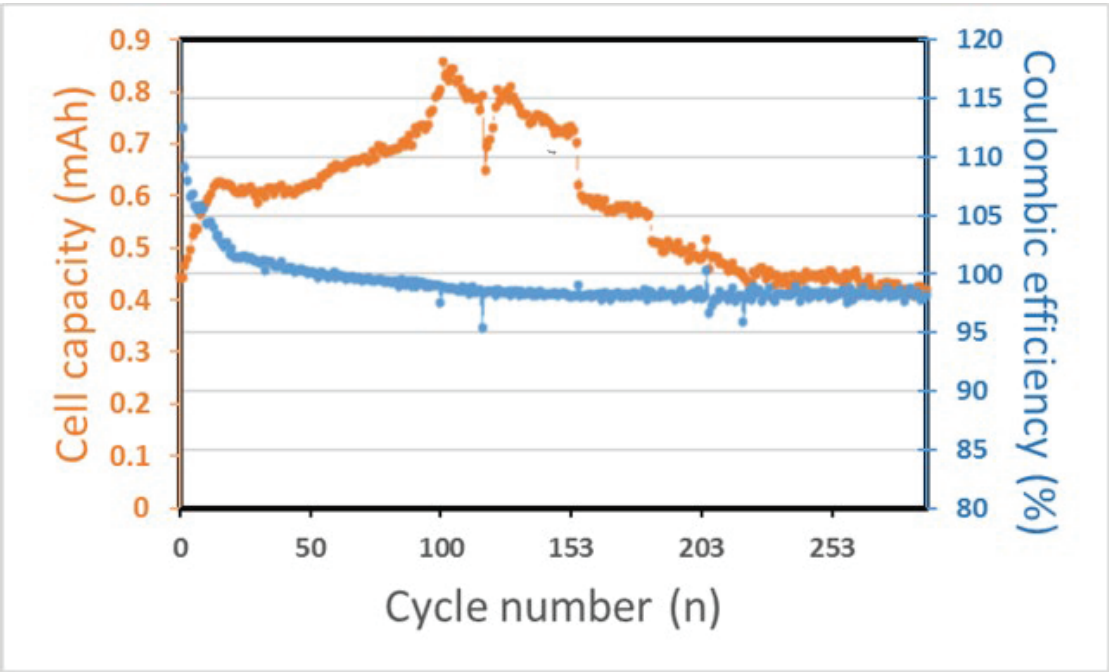

Figure 26. Cycling stability of a low capacity Lithium-Sulfur cell using hybrid electrolyte at 0.1 mA/cm^2.

Conclusions

We synthesized garnet fibrous membrane, which essentially retained the characteristic physical features of the original cellulose template and can be tailored for particular shapes in large dimensions (4 cm × 4 cm). We synthesized ion insulating polymer PEO, ion conductive polymer PEO-LiTFSI, and in-situ coated garnet nanofibers by polymer electrolyte. Our flexible electrolyte combining conductive cubic LLZO garnet and lithium-PEO acheived a reasonably high ionic conductivity of 2.5×10^{-4} S/cm at room temperature. Molecular dynamics simulations were performed to understand Li^+ diffusion in garnet nanofibers and the effect of mechanical deformation. The MD simulations in both bulk and nanofiber show mechanical deformation decreases Li^+ conductivity in garnet. We fully characterized garnet nanofiber membrane and its hybrid electrolyte for solid state lithium metal battery application. The hybrid electrolyte shows

reasonably high ionic conductivity, mechanical strength and thermal stability. We synthesized thin garnet nanofiber membrane and hybrid electrolyte with thickness of ~11 micron. Fundamental understand of the Li cycling in hybrid and other SSE are provided by both experiments and computation modeling. Our garnet nanofiber membrane reinforced hybrid was cycled at high current density of 3 mA/cm^2 for 500 cycles without lithium dendrite penetration. We used the modeling of lithium dendrite to understand lithium dendrite growth mechanism and the protection effect of polymer and interphase layers on garnet nanofiber. We fabricated porous framework of mixed electron and ion conductor as the host of S cathode in full cells and evaluated the ionic and electronic conductivity of the mixed conductor. With the hybrid electrolyte, we assembled Li-S full cells and evaluated the full cell performance. We achieved lithium-sulfur battery with a total capacity of 12.5 mAh. The full cells achieved energy density of 195 Wh/kg or 776 Wh/L.

Presentations

1. Eric Wachsman, "All-Solid-State Li-ion Batteries for Transformational Energy Storage," 21st International Conference on Solid State Ionics, June 23-29, 2017, Padua, Italy - Invited
2. Yifei Mo, "Enabling All-Solid-State Li-ion Batteries Through Computation-Guided Design of Materials and Interfaces", Beyond Lithium Ion Symposium-10 (BLI-X), CA (06/2017) - Invited
3. Yifei Mo, "Computation-Guided Understanding and Design of Interfaces in All-Solid-State Li-ion Batteries", 17th Annual Advanced Automotive Battery Conference, San Francisco, CA (06/2017)- Invited
4. Eric Wachsman, "All-Solid-State Li-ion Batteries for Transformational Energy Storage," U.C. Berkeley, April 6, 2017, Berkeley, CA – Invited
5. E. D. Wachsman, "Beyond Dendrites, Cycling Li-Metal Across Garnet at High Current Densities", Argonne National Lab, September 6, 2018, Lemont, IL
6. L. Hu, 14th Lithium Battery: Materials and Chemistries, November 1-2, 2018.
7. Y. Mo, "Computation Accelerated Design of Materials and Interfaces for Solid-State Batteries", 21st International Conference on Ternary and Multinary Compounds, September 2018, Boulder, CO (Invited)
8. Y. Mo, "Computation Accelerated Design of Materials and Interfaces for Solid-State Batteries", Applied Mechanics Seminar, Harvard University, April 2018, (Invited)
9. Y. Mo, "First-Principles Computation Study and Design for Solid Electrolyte–Electrode Interfaces in All-Solid-State Li-Ion Batteries", Materials Research Society (MRS) Spring Meeting, April 2018, Phoenix AZ (Invited)
10. Y. Mo, "Computation Accelerated Design of Materials and Interfaces for All-Solid-State Li-ion Batteries", Nature Conference on Materials Electrochemistry: Fundamentals & Applications, January 2018, Shenzhen, China (Invited)

11. X. He, Y. Mo, "Universal Strategy to Design Super-Ionic Conductors through First Principles Computation", Materials Research Society (MRS) Spring Meeting, April 201, Phoenix AZ
12. Y. Zhu, Y. Mo., "Atomistic Modeling of Interface Transport in All-Solid-State Li-ion Batteries", Materials Research Society (MRS) Spring Meeting, April 2018, Phoenix AZ
13. Y. Zhu, Y. Mo., "Novel Strategies for Lithium Metal Anode Protection from Computation-Guided Materials Discovery", Materials Research Society (MRS) Spring Meeting, April 2018, Phoenix AZ
14. Y. Mo, "Understanding Fast Ion Diffusion in Super-Ionic Conductors and Computational Materials Design", MRS Fall meeting, Boston, MA (11/2018) (Invited)
15. Y. Mo, "Design Principles for Solid Electrolyte–Electrode Interfaces in All-Solid-State Li-Ion Batteries : Insight from First-Principles Computation", MRS Fall meeting, Boston, MA (11/2018) (Invited)
16. Y. Mo, "Computation Accelerated Design of Materials and Interfaces for Solid-State Batteries", 21st International Conference on Ternary and Multinary Compounds, Boulder, CO (09/2018) (Invited)

Publications

1. K Fu et al. Flexible, solid-state, ion-conducting membrane with 3D garnet nanofiber networks for lithium batteries, *PNAS* **2016**, 113, 7094-7099.
2. Y. Gong, K. Fu, S. Xu, J. Dai, T. R. Hamann, L. Zhang, G. T. Hitz, X. Han, L. Hu, E. D. Wachsman, Lithium-Ion Conductive Ceramic Textile: A New Architecture for Flexible Solid-State Lithium Metal Batteries, Materials Today, Volume 21, 6, 594-601, 2018
3. A. Nolan, Y. Zhu, X. He, Q. Bai, Y. Mo, "Computation-Accelerated Design of Materials and Interfaces for All-Solid-State Lithium-Ion Batteries", Joule, 2, 2016-2046, 2018 (Invited Review)
4. K. H. Park, Q. Bai, D. H. Kim, D. Y. Oh, Y. Zhu, Y. Mo, Y. S. Jung, "Design Strategies, Practical Considerations, and New Solution Processes of Sulfide Solid Electrolytes for All-Solid-State Batteries", Advanced Energy Materials, 1800035, 2018 (Invited Review)
5. Q. Bai, L. Yang, H. Chen, Y. Mo, "Computational Studies of Electrode Materials in Sodium-Ion Batteries", Advanced Energy Materials, 1702998, 2018 (Invited Review)
6. Adelaide M. Nolan, Yunsheng Liu, Yifei Mo*, "Solid-State Chemistries Stable with High-Energy Cathodes for Lithium-Ion Batteries", ACS Energy Letters, 4, 2444-2451 (2019)

Project Period: 10/01/2016 - 09/30/2019

Federal Cash $1,250,000

Total Federal Expenditures 1,250,000

Total Recipient Share of Expenditures: $138,889